Purinergic Signalling (2009) 5:299–307
DOI 10.1007/s11302-009-9143-5

ORIGINAL ARTICLE

Ependymal cells along the lateral ventricle express functional $P2X_7$ receptors

Jonathan R. Genzen · Jean-Claude Platel · Maria E. Rubio · Angelique Bordey

Received: 18 December 2008 / Accepted: 26 January 2009 / Published online: 10 March 2009

Abstract Ependymal cells line the cerebral ventricles and are located in an ideal position to detect central nervous system injury and inflammation. The signaling mechanisms of ependymal cells, however, are poorly understood. As extracellular adenosine 5′-triphosphate is elevated in the context of cellular damage, experiments were conducted to determine whether ependymal cells along the mouse subventricular zone (SVZ) express functional purinergic receptors. Using whole-cell patch clamp recording, widespread expression of $P2X_7$ receptors was detected on ependymal cells based on their antagonist sensitivity profile and absence of response in $P2X_7^{-/-}$ mice. Immunocytochemistry confirmed the expression of $P2X_7$ receptors, and electron microscopy demonstrated that $P2X_7$ receptors are expressed on both cilia and microvilli. Ca^{2+} imaging showed that $P2X_7$ receptors expressed on cilia are indeed functional. As ependymal cells are believed to function as partner cells in the SVZ neurogenic niche, $P2X_7$ receptors may play a role in neural progenitor response to injury and inflammation.

Keywords Ependymal · Cerebrospinal fluid · Inflammation · ATP · Stem cell · Subventricular zone · Neurogenesis · P2X · Purinergic

Abbreviations

aCSF	Artificial cerebrospinal fluid
BBG	Brilliant blue G
BzATP	2′(3′)-*O*-(4-benzoylbenzoyl)adenosine 5′-triphosphate triethylammonium salt
$[Ca^{2+}]_i$	Intracellular Ca^{2+} concentration
DIC	Differential interference contrast
GLAST	Glutamate/aspartate transporter
MFA	Meclofenamic acid
oATP	Adenosine 5′-triphosphate-2′,3′-dialdehyde
PPADS	Pyridoxal phosphate-6-azo(benzene-2, 4-disulfonic acid) tetrasodium salt hydrate
SVZ	Subventricular zone

Introduction

Ependymal cells form an epithelial layer lining the cerebral ventricles. Functioning as a barrier between the brain parenchyma and cerebrospinal fluid (CSF), they play a role in cerebral fluid balance, toxin metabolism, and secretion [1]. Evidence has also demonstrated that ependymal cells synthesize proteins which modulate neurogenesis and/or stem cell self-renewal, such as noggin [2] and pigment epithelium-derived factor [3], thus emphasizing that ependymal cells are

J. R. Genzen
Department of Laboratory Medicine,
Yale University School of Medicine,
333 Cedar Street, P.O. Box 208035,
New Haven, CT 06520-8035, USA

J.-C. Platel · A. Bordey (✉)
Department of Neurosurgery, Yale University School of Medicine,
333 Cedar Street, FMB 422,
New Haven, CT 06520-8082, USA
e-mail: angelique.bordey@yale.edu

J.-C. Platel · A. Bordey
Department of Cellular and Molecular Physiology,
Yale University School of Medicine,
333 Cedar Street, FMB 422,
New Haven, CT 06520-8082, USA

M. E. Rubio
Department of Physiology and Neurobiology,
University of Connecticut,
TLS 102B, 75 North Eagleville Road, Unit 3156,
Storrs, CT 06269-3156, USA

important partner cells in the subventricular zone (SVZ) stem cell niche [4, 5]. Neuroblast migration is also affected by the flow of guidance molecules in the CSF—a process influenced by ependymal cell ciliary function [6].

The barrier function of ependymal cells, along with their role in the neurogenic microenvironment, suggests that elucidating ependymal cell signaling mechanisms will be paramount to understanding the full stem cell response to injury. Purinergic signaling plays an important role in central nervous system (CNS) response to inflammation, ischemia, and mechanical insult [7], and extracellular purine levels increase under injurious conditions [8–11]. Adenosine 5′-triphosphate (ATP; and its metabolites) activates numerous receptors such as the P2X family of ligand-gated ion channels and the P2Y and adenosine families of G-protein-coupled receptors.

Prior research suggests that CNS ependymal cells stain for at least one purinergic receptor, specifically $P2X_7$ [12–14]. The $P2X_7$ receptor is an ATP-gated ion channel which activates a large pore capable of passing molecules <900 Da across the plasma membrane [15–17]. While messenger RNA (mRNA) for $P2X_7$ has been detected in ependymal cells lining rat brain cerebral ventricles using *in situ* hybridization [12, 13] and X-gal staining in a mouse $P2X_7$ knockout model (with a LacZ insert) [14], there are well-known limitations regarding the use of antibodies against $P2X_7$ in CNS tissue to look for protein expression [14, 18]. In addition, functional evidence for $P2X_7$ in ependymal cells has been lacking.

In order to overcome these limitations, the present experiments use a combination of patch clamp electrophysiology, pharmacology, immunocytochemistry, electron microscopy, reverse transcriptase polymerase chain reaction (RT-PCR), and calcium imaging to provide evidence for functional $P2X_7$ receptor expression by lateral ventricle ependymal cells along the mouse SVZ. Activation of $P2X_7$ receptors may be involved in ependymal cell response to CNS injury and inflammation by inducing calcium signaling.

Materials and methods

Slice preparation Eighteen to 30-day-old CD1 (Charles River Laboratories, Wilmington, MA, USA), C57BL/6 (Jackson Laboratories, Bar Harbor, ME, USA), and $P2X_7$ knockout mice [*P2rx7*^{tm1Gab}; Jackson Laboratories; [19]] were used for experiments as indicated and in accordance with IACUC-approved protocols. Animals were anesthetized with pentabarbital (50 mg/kg). After craniotomy and dissection, horizontal brain slices (250–300 μm) were prepared in chilled (4°C) dissection solution (in mM): 83 NaCl, 73 sucrose, 2.5 KCl, 2.7 $MgCl_2$, 1.7 $CaCl_2$, 1.2 NaH_2PO_4, 10 glucose, 26 $NaHCO_3$, pH 7.4 and bubbled with 95% O_2/5% CO_2. Slices were incubated for >1 h in artificial CSF (aCSF) at room temperature (in mM): 125 NaCl, 2.5 KCl, 1 $MgCl_2$, 2 $CaCl_2$, 1.25 NaH_2PO_4, 10 glucose, and 26 $NaHCO_3$, pH 7.4 and bubbled with 95% O_2/5% CO_2.

Electrophysiology Slices were transferred to a recording chamber and superfused (~1 ml/min) with Mg^{2+}-free aCSF+ 100 μM barium and 100 μM meclofenamic acid and bubbled with 95% O_2/5% CO_2 at room temperature. Pipettes had a resistance of 9–12 MΩ when filled with internal solution (in mM): 130 KCl, 4 $MgCl_2$, 0.25 $CaCl_2$, 10 4-(2-hydroxyethyl)piperazine-1-ethanesulfonic acid (HEPES), 5 EGTA, 4 K_2ATP, 0.5 Na_2GTP, pH 7.4. Experiments were performed on an upright microscope (Olympus BX51WI, Olympus, Center Valley, PA, USA) under phase-contrast optics (×60 objective, NA 0.9). An Axopatch 200B patch clamp amplifier, Digidata 1322A digitizer, and PClamp9 software (Axon, CA, USA) were used for recordings (2 kHz low-pass filtered; 5 kHz sampling rate). Ciliated ependymal cells were visually identified along the SVZ border lining the lateral ventricle. The presence of moving cilia was an inclusion criterion for recording. Cells were maintained at a holding potential of −80 mV. Agonists were pressure applied using a Picospritzer II (2–6 psi; Parker Instrumentation). No currents were observed during puffs of aCSF alone (data not shown). Antagonists were included in both the bath solution and the pressure solution containing agonist. Clampfit 9.0 (Axon) was used to measure peak current amplitudes, which were divided by cell capacitance to determine current density (pA/pF).

Acutely dissociated ependymal cell recordings Dissection and slicing proceeded as above, except with 400 μm horizontal slices. The SVZ and ventricular wall were microdissected and collected in cold aCSF on ice. Tissue was centrifuged for 2 min at 0.3 rcf, resuspended, and dissociated using the Neural Tissue Dissociation Kit (Miltenyi Biotec Inc., Auburn, CA, USA). Cells were dissociated enzymatically and with gentle mechanical trituration. Cells were washed in DMEM and allowed to settle onto L-lysine-coated coverslips for a minimum of 1 h in a 37°C incubator with 5% CO_2 before recording at room temperature.

Genotyping $P2X7^{+/+}$ and $P2X7^{-/-}$ mice were bred as separate, homozygous colonies but are phenotypically similar. Genotyping was therefore performed on all animals used in knockout-related experiments to survey for any potential errors in animal husbandry. Tail clips were added to 200 μl 50 mM NaOH and incubated at 98°C for 1 h. To each tube, 20 μl 1 M Tris–HCl (pH 8) was then added, and samples were centrifuged for 3 min at 4,000×*g*. PCR was

conducted using the AccuPrime™ Taq DNA Polymerase System (Invitrogen) and contained in 26 μl total: 15 μl DEPC water, 2.5 μl 10× PCR buffer, 4 μl sample DNA, 0.5 μl Taq polymerase, and 1 μl each of the four genotyping primers listed in Table 1. Of note, the first primer pair amplifies a wild-type 363-bp fragment which flanks the insertion in the knockout. The second primer pair amplifies a 280-bp fragment from the neomycin resistance gene insertion used in the generation of the functional knockout. Thirty-five PCR cycles were run (94°C 30 s, 60°C 60 s, 72°C 60 s) ending with a 72°C 2-min extension and 4°C hold before the product was resolved on 2% Supra Sieve GPG/LE agarose gel in Tris–acetate–EDTA (TAE) buffer.

Immunocytochemistry Immunocytochemistry was performed according to previously described protocols [20]. Primary antibodies included 1:100 rabbit anti-$P2X_7$ (#AB5246) and 1:500 guinea pig anti-GLAST (Chemicon, MA, USA), 1:100 rabbit anti-S100β (Sigma, MO, USA), and 1:100 goat anti-doublecortin (Santa Cruz, CA, USA). One hundred-micrometer slices were washed with 0.05 M tris base in 9% NaCl at pH 7.4 (Tris-buffered saline—TBS), permeabilized in TBS+0.1% Triton X-100 (TBST), blocked in TBST+10% normal donkey serum, and then incubated overnight with primary antibody at 4°C. After washing (3×45 min in TBST), slices were incubated 2 h at RT in secondary antibody solution (donkey, Alexa Fluor ® 488, 594, 633, and/or 647; Invitrogen). After 3×30-min washes in TBS, they were mounted on coverslips with Prolong® Gold Antifade Reagent (Invitrogen) with or without 1:1,000 DAPI.

Freeze substitution and postembedding immunogold labeling For the detection of $P2X_7$ receptor subunit by electron microscopy with immunogold labeling after freeze substitution, a protocol similar to that described in detail elsewhere was used [21]. Briefly, using P22 CD1 mice, coronal sections at the level of the subventricular zone were dissected and processed for freeze substitution and low-temperature embedding. For postembedding immunocytochemistry, ultrathin sections (80 nm in thickness) on nickel grids were incubated in sodium borohydride and glycine in Tris-buffered saline solution with Triton X-100. After being pre-blocked with serum, the sections were incubated with the affinity-purified primary polyclonal antibody for $P2X_7$ (1.5 μg; Alomone Labs, Jerusalem, Israel; same epitope as $P2X_7$ antibody described above, #APR-004). Primary antibody was detected with a secondary antibody conjugated to 5-nm gold particles in diameter (1:20; Amersham GE Healthcare, Buckinghamshire, UK). No gold particles were observed on mitochondria and myelin sheets. Control sections were prepared in the absence of the primary antibody during the incubation step. No gold particles were observed on the ultrathin sections after the control procedure. Ultrathin sections were analyzed with a TECNAI G2 Spirit Biotwin transmission electron microscope (FEI Company, Hillsboro, OR, USA). The images were captured with a CCD camera (Advanced Microscopy Techniques, Danvers, MA, USA) at ×49,000, ×68,000, or ×98,000 magnification. Image processing was performed with Adobe Photoshop (Adobe Systems, San Jose, CA, USA) using only the brightness and contrast commands to enhance gold particles.

Reverse transcriptase polymerase chain reaction Ten cell aspirates of ependymal cells from horizontal slices were made using RNase-free internal solution [150 mM KCl, 10 mM HEPES, 0.5 U/μl RNase inhibitor (Invitrogen)]. Cells were aspirated and solution was ejected in 5 μl RNase-free water containing an additional 1 μl 10 mM dNTP and 1 μl random hexamers (50 ng/μl). RT master mix from the SuperScript™ III First-Strand Synthesis System for RT-PCR (Invitrogen) was added, and contained 2 μl 10× PCR buffer, 4 μl 25 mM $MgCl_2$, 2 μl 0.1 M DTT, 1 μl 40 U/ml RNAseOUT, and a reverse transcription protocol was run (25°C 10 min, 50°C 50 min, 85°C 5 min). Samples were treated with RNaseH for 20 min at 37°C then kept on ice until PCR. PCR was conducted using the AccuPrime™ Taq DNA Polymerase System (Invitrogen) and contained in 50 μl total: 25 μl DEPC water, 5 μl 10× PCR buffer, 18 μl cDNA template, 1 μl Taq polymerase,

Table 1 Primers used in RT-PCR of ependymal cells and animal genotyping

Target	Primer	Basic *T*(m), °C	Product size (bp)	Restriction enzyme (cleaved sizes in bp)
RT-PCR				
P2X7	5′ TCTTCCGACTAGGGGACATCT 3′	54	119	*Bgl*II (82, 37)
	5′ ATGGGACCAGCTGTCTAGGTT 3′	54		
Genotyping				
P2X7+/+	5′ TGGACTTCTCCGACCTGTCT 3′	54	363	n.a.
	5′ TGGCATAGCACCTGTAAGCA 3′	52		
P2X7−/−	5′ CTTGGGTGGAGAGGCTATTC 3′	54	280	n.a.
(neo insert)	5′ AGGTGAGATGACAGGAGATC 3′	52		

and 0.5 μl each of P2X7 primers (Table 1, RT-PCR primers). Thirty-five PCR cycles were run (94°C 30 s, 55°C 30 s, 68°C 1 min), 4 μl PCR product was added to fresh mastermix and primer, and an additional 20 PCR cycles were run. Product was resolved on 4% Supra Sieve GPG agarose gel (American Bioanalytical, Natick, MA, USA) in TAE buffer and photographed using a Kodak GelLogic Digital Imaging System (New Haven, CT, USA). For restriction enzyme analysis, PCR product was purified using a Qiaquick PCR Purification Kit (Qiagen, Valencia, CA, USA) before a 20-min 65°C incubation in *Bgl*II restriction enzyme (New England Biolabs, Ipswich, MA, USA).

Calcium imaging Acute mouse brain slices were loaded for 30 min at 37°C with the Ca^{2+}-sensitive dye Fluo-4AM (Invitrogen; 4 μM in DMSO with 20% Pluronic F-127), then washed for a minimum of 30 min before recording. Later experiments were conducted using focal, ependyma-directed pressure application of Fluo-4AM or Oregon Green BAPTA-1AM (Invitrogen) dissolved in Pluronic F-127, which yielded equivalent loading of ependyma with improved tissue viability. Slices were washed for a minimum of 10 min before recording. The Ca^{2+} imaging system consisted of a confocal laser scanning microscope (Olympus) with a ×60 water objective (NA 0.9) and Fluoview software. Calcium data were analyzed using the Calsignal program [22].

Reagents Salts used for aCSF and pipette solutions, as well as ATP, brilliant blue G, 2′(3′)-*O*-(4-benzoylbenzoyl)adenosine 5′-triphosphate triethylammonium salt (BzATP), GTP, adenosine 5′-triphosphate-2′,3′-dialdehyde (oATP), and pyridoxal phosphate-6-azo(benzene-2,4-disulfonic acid) tetrasodium salt hydrate (PPADS) were purchased from Sigma (St. Louis, MO, USA).

Statistics Data were analyzed and presented in SigmaPlot 8.0 (SPSS, Chicago, IL, USA). Statistical significance was determined using the Student's *t* test ($p<0.05$). Data are presented as mean ± SEM unless otherwise indicated.

Results

Ependymal cells express functional P2X$_7$ receptors Unambiguous identification of ependymal cells was first confirmed using immunocytochemistry of the SVZ. As shown in Fig. 1a, S100β-positive ependymal cells line the walls of the lateral ventricles and can be found near the glutamate/aspartate transporter (GLAST)-positive astrocytes and doublecortin-positive neuroblasts (see inset *a′* for slice orientation). In acute, live horizontal slices of CD1 mouse brain (age 18–30 days), the presence of motile cilia was used to identify ependymal cells along the lateral ventricle surface of the SVZ for subsequent whole-cell patch clamp recordings (Fig. 1b). Ependymal cells displayed a resting membrane potential (V_m) of −76.8±1.0 mV (n=50 cells), consistent with prior observations from the literature and our laboratory [20, 23]. Voltage step experiments confirmed that ependymal cells have currents sensitive to 100 μM Ba^{2+}, consistent with inwardly rectifying K^+ channels (Fig. 1c, d) [20].

Pressure application of agonists demonstrated that 100% of cells responded to BzATP (n=29/29; concentration range, 100–1,000 μM). Inward currents induced by BzATP were larger than currents induced by equimolar concentrations of ATP (Fig. 1e), an observation also seen in concentration-response experiments (Fig. 1f; n=2–12 cells per dose). Prolonged application of BzATP resulted in currents with an initial rapid component, then a larger second component displaying a linear increase in current amplitude over the 60-s application (Fig. 1g).

BzATP-induced responses in ependyma were reduced by pre-incubation with the P2X$_7$ receptor antagonist oATP (Fig. 2a, 300 μM). The antagonist profile was also consistent with P2X$_7$, including block by PPADS, oATP, brilliant blue G (BBG), but not suramin (Fig 2b; n=9–11 cells per condition, $*p<0.05$). BzATP-induced responses were also blocked by divalent cations such as Zn^{2+}, Mg^{2+}, and Cu^{2+} (Fig 2c; n=5–12 cells per condition, $*p<0.05$). BzATP-induced currents at a physiological Mg^{2+} concentration (0.8 mM, 4.8±1.2 pA/pF; n=5) were smaller than those observed in the absence of Mg^{2+} (13.6±1.9 pA/pF; n=10, $*p<0.05$), but were still detectable and significantly larger than in the presence of 10 mM Mg^{2+} (0.5±0.3 pA/pF; n=12; $*p<0.05$). This suggests that P2X$_7$ receptors on ependymal cells are functional at physiological Mg^{2+} concentrations. mRNA for the P2X$_7$ receptor was also

Fig. 1 Localization and patch-clamp recording of lateral ventricle ependymal cells: purinergic responses. **a** Triple-labeled immunocytochemistry demonstrating the localization of S100β-positive ependymal cells [*green*] along the lateral ventricle in CD1 mice. Subependymal GLAST-positive type-B astrocytes [*red*] and doublecortin-positive neuroblasts [*blue*] can also be seen along the SVZ (bar=25 μm). *Inset* (*a′*) shows the relative location of the SVZ in a horizontal slice of mouse brain. **b** DIC image of ependymal cells lining the wall of the lateral ventricle in an acute mouse brain slice (bar=25 μm). The position of recording and pressure pipettes is indicated. **c** Current responses to voltage steps (−180 to +120 mV) in the absence and presence of Ba^{2+} (bar=1 nA, 100 ms). **d** Current/voltage plot derived from the cell in (**c**) in the presence and absence of Ba^{2+} with subtraction current. **e** Ten-second application of BzATP induced a rapid inward current in ependymal cells from CD1 mice. Application of equimolar ATP onto the same cell induced a smaller current (bar=100 pA, 3 s). **f** Summary histogram of concentration-response experiments demonstrating relative potency of BzATP versus ATP on ependymal cells (n=2–12 cells per dose). **g** Prolonged (60 s) application of BzATP resulted in an initial, rapidly activating inward current, but also a larger second component with a linear increase in current amplitude (bar=150 pA, 10 s)

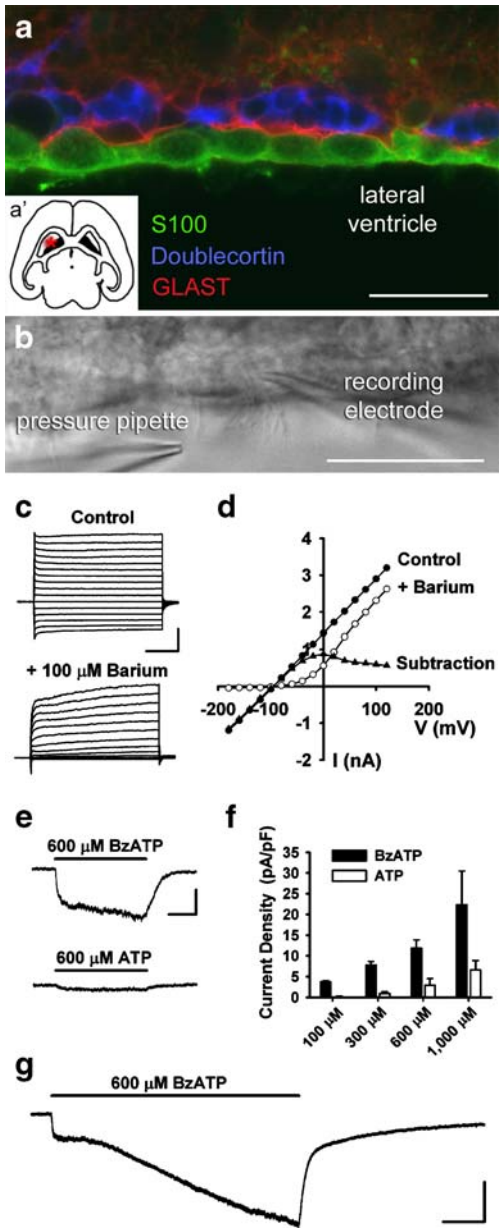

detected with RT-PCR of ependymal cell aspirates from acute slices (Fig. 2d).

As it is theoretically possible that $P2X_7$ receptor-mediated responses in ependymal cells could be due to activation of neighboring cells leading to indirect effects on ependyma, patch clamp recordings were conducted using acutely dissociated ependymal cells (Fig. 2e–g). BzATP-induced currents were observed in isolated ependymal cells, and this response was blocked by Mg^{2+}, consistent with $P2X_7$ receptor expression by ependymal cells.

BzATP-induced currents are absent in ependymal cells of $P2X_7^{-/-}$ mice In order to determine whether BzATP responses are absent in a $P2X_7$ receptor knockout model, we acquired $P2X_7^{-/-}$ mice [*P2rx7*^{tm1Gab}; Jackson Laboratories; [19]] and compared them to C57BL/6 ($P2X_7^{+/+}$) controls. PCR confirmed the genotype in all mice used for the experiments (Fig. 3a). Whole-cell patch clamping revealed that prolonged application of BzATP-induced currents in the $P2X_7^{+/+}$ animals (Fig. 3b) but not $P2X_7^{-/-}$ animals (Fig. 3c). Figure 3d summarizes these data from all cells tested in $P2X_7^{+/+}$ mice (9.0±1.1 pA/pF, n=8 cells from two animals) and $P2X_7^{-/-}$ mice (0.01±0.06 pA/pF, n=16 cells from four animals, *p<0.05). It should be noted that in $P2X_7^{-/-}$ mice, 1 mM ATP (n=10 cells) did not induce any inward currents (data not shown), thus there is no evidence for compensatory expression of another P2X receptor/ATP-gated ion channel. Finally, ependymal $P2X_7$ immunoreactivity (green) was present in $P2X_7^{+/+}$ mice (Fig. 3e) but not $P2X_7^{-/-}$ mice (Fig. 3f). Ependymal $P2X_7$ immunoreactivity was also observed in 5- and 14-month-old $P2X_7^{+/+}$ animals (data not shown), demonstrating that $P2X_7$ receptor expression is not limited to the neonatal or adolescent period. No $P2X_7$ immunoreactivity was observed in SVZ astrocytes or neuroblasts.

Electron microscopy was performed to examine the subcellular localization of the $P2X_7$ receptors on ependymal cells. Immunogold labeling was observed on ependymal cells but not SVZ astrocytes or neuroblasts (Fig. 4a–d) consistent with the immunohistochemistry outlined above. Figure 4 shows that gold particles were frequently observed along the plasma membrane of cilia (Fig. 4e, f) and microvilli (Fig. 4g, h). Intracellular immunogold labeling was also observed in ependymal cells (data not shown). Immunogold particle counting in 35 fields (1,063× 1,063 nm) along the ependymal surface revealed a density of 3.0±0.7 particles/μm length of cilia and 1.2±0.4 particles/μm length of microvilli (cilia versus microvilli comparison, p=0.08; data not shown).

Activation of $P2X_7$ leads to increases in intracellular Ca^{2+} In order to determine whether somatic and ciliary $P2X_7$ receptor activation may be involved in mediating intracellular Ca^{2+} ($[Ca^{2+}]_i$) changes, ependymal cells were loaded with either Fluo-4AM (Fig. 5a) or Oregon Green BAPTA-1AM and exposed to low-pressure applications of 600 μM BzATP. Marked increases in $[Ca^{2+}]_i$ were observed during BzATP application (Fig. 5c) as compared to baseline (Fig. 5b). Loaded cilia (marked by asterisks in Fig. 5c) were often difficult to visualize under baseline conditions but were easily observed in the presence of BzATP. Ninety-four percent of lateral ventricle ependymal cells (n=4–6 cells per slice, eight CD1 slices) responded to BzATP with increases in $[Ca^{2+}]_i$. As expected, increases in $[Ca^{2+}]_i$ were also observed in 96% of ependymal cells in the C57BL/6 ($P2X_7^{+/+}$) mice during BzATP application (Fig. 5d, f, g). $[Ca^{2+}]_i$ changes in $P2X_7^{-/-}$ mice, however, were largely eliminated in both prevalence (6%) and amplitude

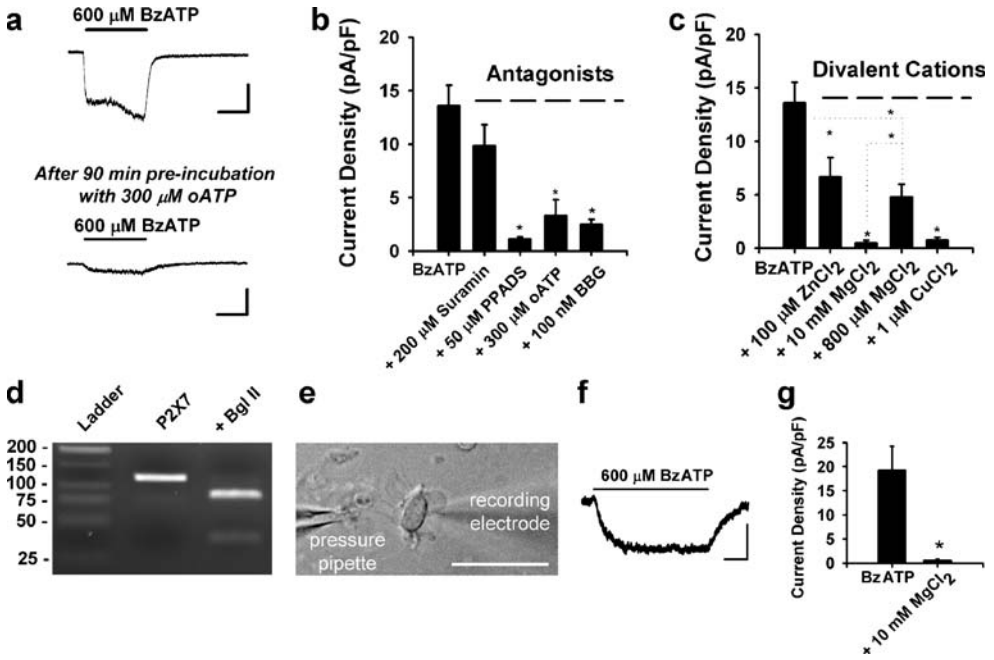

Fig. 2 Ependymal cells express functional $P2X_7$ receptors. **a** Response to BzATP application is reduced after 90-min pre-incubation with 300 μM oATP (data from separate cells; bars=100 pA, 5 s). **b** Summary histogram showing antagonist effects on 600 μM BzATP-induced currents. Consistent with $P2X_7$ responses in other studies, BzATP-induced currents (13.6±1.9 pA/pF; n=10) were not significantly blocked by 200 μM suramin (9.9±2.0 pA/pF; n=10, p=0.19), but were significantly attenuated by 50 μM PPADS (1.1±0.2 pA/pF; n=9), 300 μM oATP (3.3±1.5 pA/pF; n=11), and 100 nM BBG (2.5±0.5 pA/pF; n=10). **c** Summary histogram demonstrating reduction of BzATP-induced currents by 100 μM Zn^{2+} (6.7±1.8 pA/pF; n=9), 10 mM Mg^{2+} (0.5±0.3 pA/pF; n=12), 800 μM Mg^{2+} (4.8±1.2 pA/pF; n=5), and 1 μM Cu^{2+} (0.7±0.3 pA/pF; n=10). **d** Agarose gel electrophoresis demonstrating RT-PCR amplification of $P2X_7$ mRNA isolated during pipette aspiration of cytoplasm from ten ependymal cells directly lining the SVZ. Product of 119 bp was identified. The restriction endonuclease *Bgl*II (AGATCT) cleaved the amplified product to the predicted sizes of 82 and 37 bp. $P2X_7$ was not detected in bath or water controls and bands corresponding to genomic $P2X_7$ (1,588 bp) were never observed. **e** DIC image of an acutely dissociated ependymal cell during whole-cell patch clamp recording. Cells were identified based on the presence of moving cilia (bar=25 μm). **f** Representative trace showing an inward current induced by 600 μM BzATP in this acutely dissociated cell (bar=200 pA, 2 s). **g** Summary histogram showing the average current density of BzATP-induced responses in acutely dissociated cells (19.3±5.0 pA/pF; n=5) and in the presence of 10 mM Mg^{2+} (0.6±0.3 pA/pF; n=4). *p<0.05 for panels **b**, **c**, and **g**)

(Fig. 5e, f, g). Due to the enhanced visualization of cilia during BzATP application (Fig. 5c), we used a higher acquisition speed (30 Hz) and ×6 digital zoom in subsequent experiments (Fig. 5h, i) to look at the time course of $[Ca^{2+}]_i$ changes in cilia (Fig. 5i, dotted boxes) versus ependymal cell soma (Fig. 5i, solid boxes). As shown in Fig. 5j, increases in $[Ca^{2+}]_i$ occurred simultaneously in the cilia and soma, providing evidence that $P2X_7$ expressed on cilia are indeed functional.

Discussion

The present experiments demonstrate that lateral ventricle ependymal cells in mice express the ligand-gated ion channel $P2X_7$. Receptor activation leads to increases in $[Ca^{2+}]_i$. While electrophysiological experiments in $P2X_7^{-/-}$ mice did not reveal any additional P2X receptor in ependymal cells, the present results do not preclude the possibility of additional purinergic receptors that are not coupled to ionic currents or Ca^{2+} changes.

Prior identification of $P2X_7$ receptor expression by ependymal cells has largely been hindered by well-described problems associated with antibody-based approaches in assigning $P2X_7$ reactivity in the CNS [14, 18]. These problems are likely due to a persistent non-$P2X_7$ epitope in $P2X_7^{-/-}$ mice and/or the presence of a $P2X_7$-like protein. In accordance, we observed significant background staining in both $P2X_7^{+/+}$ and $P2X_7^{-/-}$ strains using an anti-$P2X_7$ C-terminus antibody, especially on blood vessels (data not shown). Differences in immunoreactivity, however, were readily apparent on ependyma. While in control experiments all staining was eliminated by a supplied blocking peptide for $P2X_7$, this only demonstrates that the epitope binding sites on the antibody were saturated. Our patch-clamp experiments, however, confirm that in $P2X_7^{-/-}$ mice there are no functional $P2X_7$ receptors on ependymal cells, nor is there any evidence for a receptor with a shared pharmacological profile or other P2X-like characteristics. It should also be noted that the pharmacology of our $P2X_7$ receptors differs from the previously characterized $P2X_{cilia}$

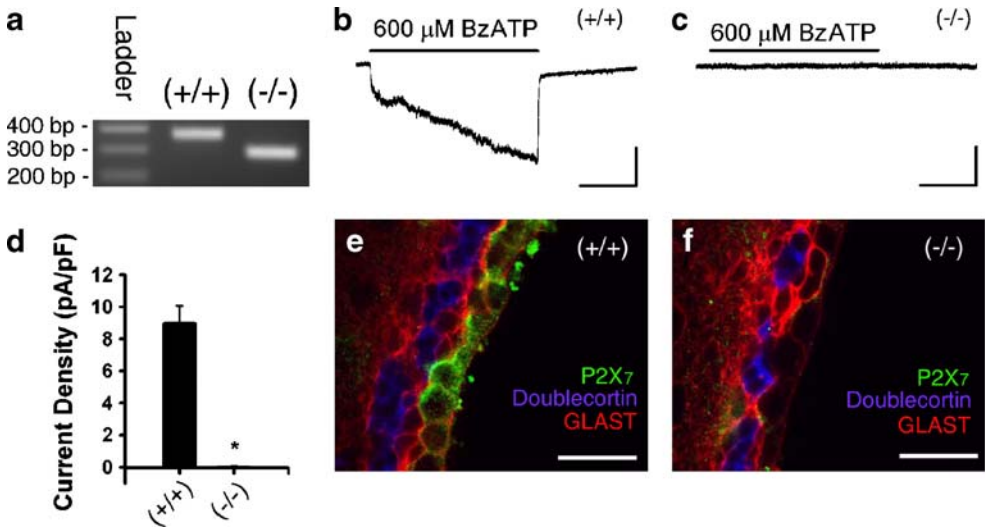

Fig. 3 Ependymal cell response to BzATP is absent in $P2X_7^{-/-}$ mice. **a** The genotype of C57Bl/6 ($P2X_7^{+/+}$) and $P2X_7^{-/-}$ mice was confirmed by PCR [(+/+) 363 bp, (−/−) 280 bp]. CD1 wild-type mice also show a 363-bp product (data not shown). **b**, **c** Prolonged (60 s) applications of BzATP induce inward currents in $P2X_7^{+/+}$ (**b**) but not $P2X_7^{-/-}$ (**c**) mice (bars=100 pA, 20 s). **d** Summary histogram showing the average current density of BzATP-induced responses in $P2X_7^{+/+}$ mice (9.0± 1.1 pA/pF; n=8) and lack of currents induced in $P2X_7^{-/-}$ mice (0.01± 0.06 pA/pF; n=16, *p<0.05). **e**, **f** Ependymal $P2X_7$ immunoreactivity (*green*) is present in $P2X_7^{+/+}$ mice (**e**) but is absent in $P2X_7^{-/-}$ mice (**f**). Also shown are GLAST (*red*) and doublecortin (*blue*; bar=25 μm)

Fig. 4 $P2X_7$ receptors are expressed on ependymal cells but not subventricular zone astrocytes or neuroblasts. **a** Transmission electron micrograph of the SVZ at low magnification showing the location of subsequent insets of an astrocyte (**b**), ependymal cell (**c**), and neuroblast (**d**; bar=10 μm). **b**–**d** Immunogold labeling for $P2X_7$ was not observed in astrocytes or neuroblasts but was evident in ependymal cells (bars=500 nm). (**c′**) Higher power inset showing $P2X_7$ labeling (*arrows*) along the plasma membrane of an ependymal cell (bars=100 nm). **e**–**h** Electron micrographs demonstrating immunogold labeling for $P2X_7$ on the surface of cilia (**e**, **f**) and microvilli (**g**, **h**; bar=100 nM)

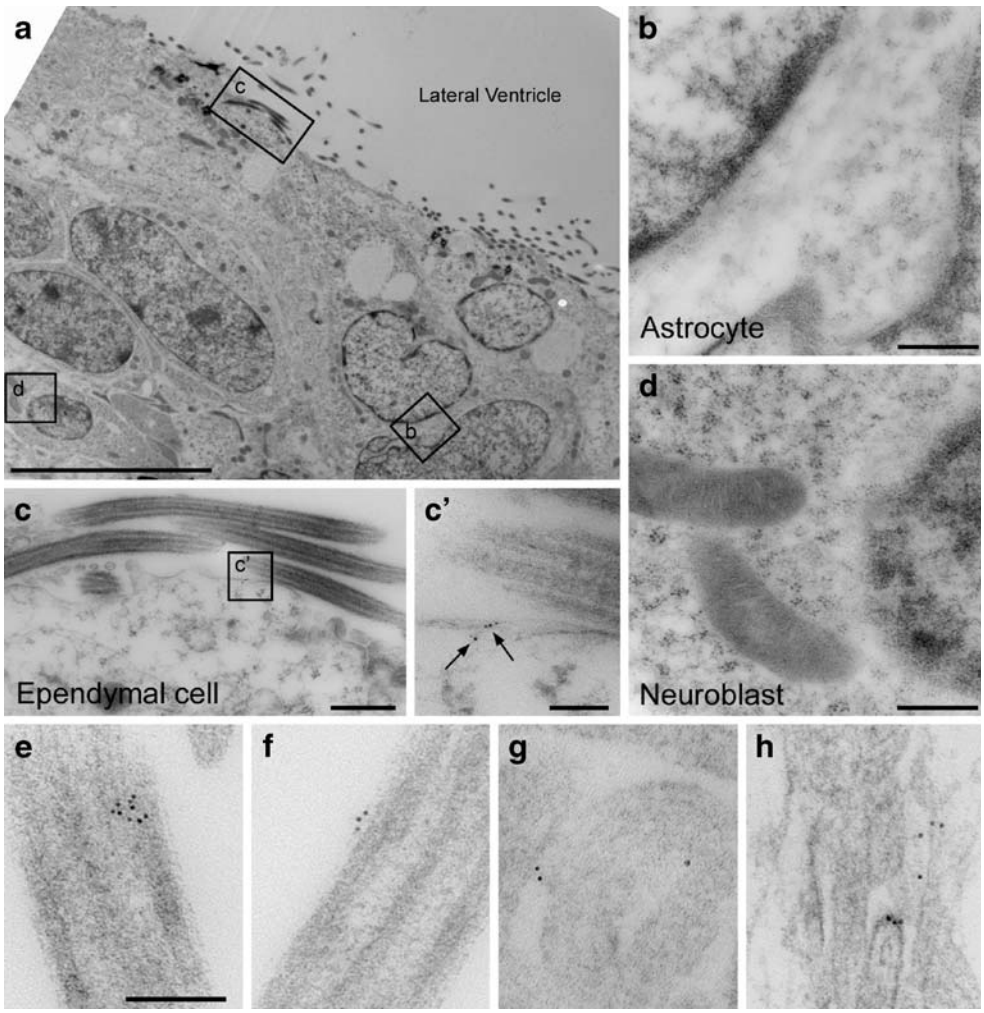

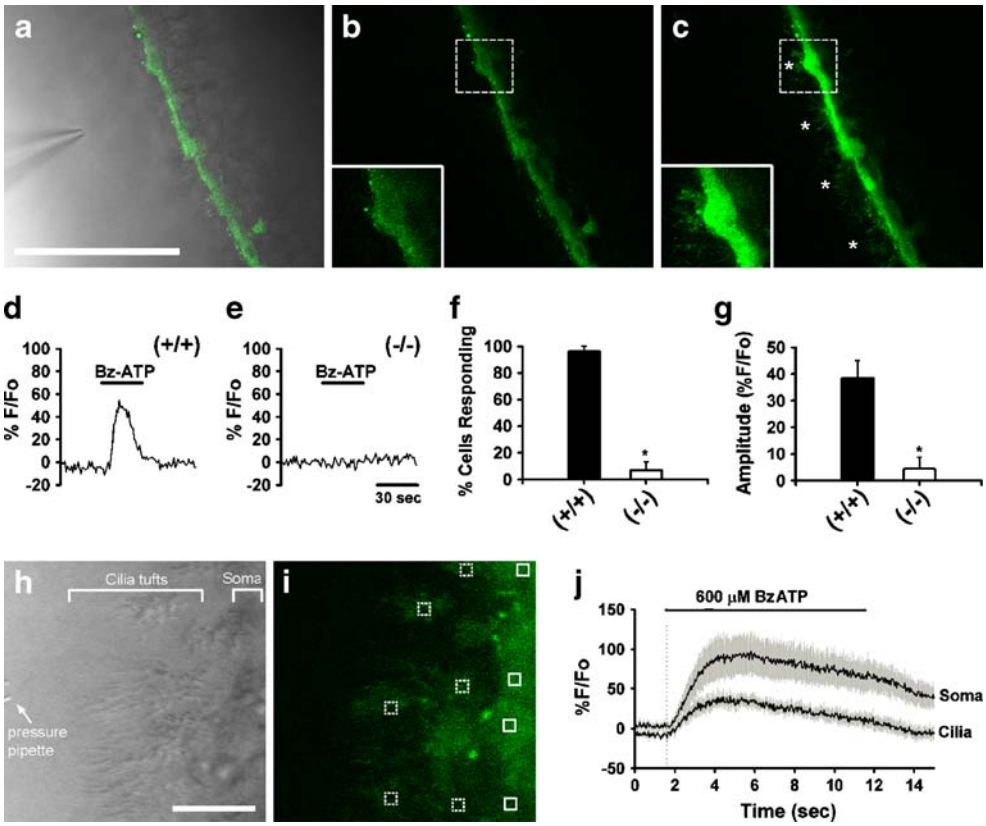

Fig. 5 Activation of ependymal $P2X_7$ receptors results in intracellular calcium increases. **a** Combined DIC and Fluo-4-AM image showing loaded ependymal cells (bar=50 μm). Intracellular $[Ca^{2+}]$ increased from baseline level (**b**) during pressure application of 600 μM BzATP (**c**). *Insets* shown in (**b**) and (**c**) are ×2 digital zooms of regions indicated by the *dashed boxes*. Increases in $[Ca^{2+}]$ were evident in cilia (*asterisks*) during BzATP application. $[Ca^{2+}]_i$ increases were also evident during 600 μM BzATP application onto ependymal cells of $P2X_7^{+/+}$ mice (**d**) but not in the $P2X_7^{-/-}$ mice (**e**). **f** Summary histogram of response prevalence in $P2X_7^{+/+}$ versus $P2X_7^{-/-}$ animals. **g** Summary histogram of response amplitude in $P2X_7^{+/+}$ (average % F/F_o=38.5±6.5; n=5 slices) versus $P2X_7^{-/-}$ (average % F/F_o=4.4±4.4; n=5 slices) animals. **h** DIC image showing a high magnification view of a pressure pipette positioned near tufts of cilia and ependymal cell bodies (bar=10 μm). **i** The corresponding image of the loaded slice (Oregon Green) with multiple areas of interest over ciliary tufts (*dotted boxes*) and soma (*solid boxes*). **j** High-speed acquisition (30 Hz) of fluorescence changes revealed that increases in $[Ca^{2+}]_i$ during BzATP application occur simultaneously in cilia and the ependymal cell soma

(a likely $P2X_4/P2X_7$ combination found in rabbit airway cells) as the ependymal $P2X_7$ response is reduced by Zn^{2+} while suramin has no appreciable effect [24].

Electron microscopy and immunocytochemistry demonstrated that $P2X_7$ receptors were found along ependymal cell cilia and microvilli, but not in neuroblasts or astrocytes. Rare intra-cilia labeling also suggested transport of receptors. Given the previously discussed limitations of $P2X_7$ immunocytochemistry, we also used a confocal-based Ca^{2+} imaging approach to verify functional expression of $P2X_7$ on cilia and the ependymal soma. Time comparison (millisecond scale) of Ca^{2+} increases after BzATP application revealed no differences between the onset of $[Ca^{2+}]_i$ changes in cilia and the cell body, suggesting that the ciliary calcium increase is not an indirect response due to somatic $P2X_7$ receptor activation. It should be noted that no spontaneous calcium transients were observed along ependymal cells in these recordings—a sharp contrast to spontaneous activity frequently observed in the underlying SVZ [25].

The downstream implication of this enhanced Ca^{2+} signaling in ependymal cells is not clear, however. Recent evidence demonstrating regenerative repair in the ependymal layer from astrocytes [26] suggests that active signaling processes may be involved in maintaining a viable ependymal layer in health and during pathologic injury. Involvement of purinergic signaling and/or Ca^{2+}-mediated second messenger pathways in initiating such repair is one intriguing possibility.

Acknowledgments The authors thank Daniel Balkin as well as Jackson Laboratories for primer design. This work was supported by grants from the National Institute of Health R01 NS048256 and DC007681 (A.B.) and 2T32HL007974-05 (J.R.G.).

References

1. Del Bigio MR (1995) The ependyma: a protective barrier between brain and cerebrospinal fluid. Glia 14:1–13. doi:10.1002/glia.440140102
2. Lim DA, Tramontin AD, Trevejo JM et al (2000) Noggin antagonizes BMP signaling to create a niche for adult neurogenesis. Neuron 28:713–726. doi:10.1016/S0896-6273(00)00148-3
3. Ramírez-Castillejo C, Sánchez-Sánchez F, Andreu-Agulló C et al (2006) Pigment epithelium-derived factor is a niche signal for neural stem cell renewal. Nat Neurosci 9:331–339. doi:10.1038/nn1657
4. Genzen JR, Bordey A (2009) Ependymal cells and the neurogenic niche. In: Bonfanti L (ed) Postnatal and adult neurogenesis. Kerala, India, Research Signpost (in press)
5. Ohlstein B, Kai T, Decotto E et al (2004) The stem cell niche: theme and variations. Curr Opin Cell Biol 16:693–699. doi:10.1016/j.ceb.2004.09.003
6. Sawamoto K, Wichterle H, Gonzalez-Perez O et al (2006) New neurons follow the flow of cerebrospinal fluid in the adult brain. Science 311:629–632. doi:10.1126/science.1119133
7. Franke H, Krugel U, Illes P (2006) P2 receptors and neuronal injury. Pflugers Arch 452:622–644. doi:10.1007/s00424-006-0071-8
8. Juranyi Z, Sperlagh B, Vizi ES (1999) Involvement of P2 purinoceptors and the nitric oxide pathway in [3H] purine outflow evoked by short-term hypoxia and hypoglycemia in rat hippocampal slices. Brain Res 823:183–190. doi:10.1016/S0006-8993(99)01169-5
9. Wallman-Johansson A, Fredholm BB (1994) Release of adenosine and other purines from hippocampal slices stimulated electrically or by hypoxia/hypoglycemia. Effect of chlormethiazole. Life Sci 55:721–728. doi:10.1016/0024-3205(94)00680-6
10. Cunha RA, Vizi ES, Ribeiro JA et al (1996) Preferential release of ATP and its extracellular catabolism as a source of adenosine upon high- but not low-frequency stimulation of rat hippocampal slices. J Neurochem 67:2180–2187
11. Franke H, Grummich B, Hartig W et al (2006) Changes in purinergic signaling after cerebral injury—involvement of glutamatergic mechanisms? Int J Dev Neurosci 24:123–132. doi:10.1016/j.ijdevneu.2005.11.016
12. Collo G, Neidhart S, Kawashima E et al (1997) Tissue distribution of the P2X7 receptor. Neuropharmacology 36:1277–1283. doi:10.1016/S0028-3908(97)00140-8
13. Yu Y, Ugawa S, Ueda T et al (2008) Cellular localization of P2X7 receptor mRNA in the rat brain. Brain Res 1194:45–55. doi:10.1016/j.brainres.2007.11.064
14. Sim JA, Young MT, Sung HY et al (2004) Reanalysis of P2X7 receptor expression in rodent brain. J Neurosci 24:6307–6314. doi:10.1523/JNEUROSCI.1469-04.2004
15. Surprenant A, Rassendren F, Kawashima E et al (1996) The cytolytic P2Z receptor for extracellular ATP identified as a P2X receptor (P2X7). Science 272:735–738. doi:10.1126/science.272.5262.735
16. Virginio C, Church D, North RA et al (1997) Effects of divalent cations, protons and calmidazolium at the rat P2X7 receptor. Neuropharmacology 36:1285–1294. doi:10.1016/S0028-3908(97)00141-X
17. Pelegrin P, Surprenant A (2006) Pannexin-1 mediates large pore formation and interleukin-1beta release by the ATP-gated P2X7 receptor. EMBO J 25:5071–5082. doi:10.1038/sj.emboj.7601378
18. Anderson CM, Nedergaard M (2006) Emerging challenges of assigning P2X7 receptor function and immunoreactivity in neurons. Trends Neurosci 29:257–262. doi:10.1016/j.tins.2006.03.003
19. Solle M, Labasi J, Perregaux DG et al (2001) Altered cytokine production in mice lacking P2X(7) receptors. J Biol Chem 276:125–132. doi:10.1074/jbc.M006781200
20. Liu X, Bolteus A, Balkin D et al (2006) GFAP-expressing progenitors in mouse postnatal subventricular zone display a unique glial phenotype intermediate between radial glia and astrocytes. Glia 54:394–410. doi:10.1002/glia.20392
21. Rubio ME (2006) Redistribution of synaptic AMPA receptors at glutamatergic synapses in the dorsal cochlear nucleus as an early response to cochlear ablation in rats. Hear Res 216–217:154–167. doi:10.1016/j.heares.2006.03.007
22. Platel JC, Dupuis A, Boisseau S et al (2007) Synchrony of spontaneous calcium activity in mouse neocortex before synaptogenesis. Eur J Neurosci 25:920–928. doi:10.1111/j.1460-9568.2007.05367.x
23. Nguyen T, Chin WC, O'Brien JA et al (2001) Intracellular pathways regulating ciliary beating of rat brain ependymal cells. J Physiol 531:131–140. doi:10.1111/j.1469-7793.2001.0131j.x
24. Ma W, Korngreen A, Weil S et al (2006) Pore properties and pharmacological features of the P2X receptor channel in airway ciliated cells. J Physiol 571:503–517. doi:10.1113/jphysiol.2005.103408
25. Platel JC, Lacar B, Bordey A (2007) GABA and glutamate signaling: homeostatic control of adult forebrain neurogenesis. J Mol Histol 38:602–610
26. Luo J, Shook BA, Daniels SB et al (2008) Subventricular zone-mediated ependyma repair in the adult mammalian brain. J Neurosci 28:3804–3813. doi:10.1523/JNEUROSCI.0224-08.2008